Measurement of the beam asymmetry in η–photoproduction off the proton

D. Elsner[1], A.V. Anisovich[2,3], G. Anton[4], J.C.S. Bacelar[5], B. Bantes[1], O. Bartholomy[2], D. Bayadilov[2,3], R. Beck[2], Y.A. Beloglazov[3], R. Bogendörfer[4], R. Castelijns[5], V. Crede[2,6], H. Dutz[1], A. Ehmanns[2], K. Essig[2], R. Ewald[1], I. Fabry[2], H. Flemming[7], K. Fornet-Ponse[1], M. Fuchs[2], C. Funke[2], R. Gothe[1,a], R. Gregor[9], A.B. Gridnev[3], E. Gutz[2], S. Höffgen[1], P. Hoffmeister[2], I. Horn[2], J. Hössl[4], I. Jaegle[8], J. Junkersfeld[2], H. Kalinowsky[2], S. Kammer[1], V. Kleber[1], Frank Klein[1], Friedrich Klein[1], E. Klempt[2], H. Koch[7], M. Konrad[1], B. Kopf[7], M. Kotulla[8,9], B. Krusche[8], M. Lang[2], J. Langheinrich[1,b], H. Löhner[5], I.V. Lopatin[3], J. Lotz[2], S. Lugert[9], H. Matthäy[7], D. Menze[1], T. Mertens[8], J.G. Messchendorp[5], V. Metag[9], C. Morales[1], M. Nanova[9], V.A. Nikonov[2,3], D. Novinski[2,3], R. Novotny[9], M. Ostrick[1,c], L.M. Pant[9,d], H. van Pee[2,9], M. Pfeiffer[9], A. Radkov[3], A.V. Sarantsev[2,3], S. Schadmann[9,e], C. Schmidt[2], H. Schmieden[1], B. Schoch[1], S. Shende[5], G. Suft[4], A. Süle[1], V.V. Sumachev[3], T. Szczepanek[2], U. Thoma[2,9], D. Trnka[9], D. Walther[1], C. Weinheimer[2,f], and C. Wendel[2]
(The CBELSA/TAPS collaboration)

[1] Physikalisches Institut der Universität Bonn, Germany
[2] Helmholtz-Institut für Strahlen- und Kernphysik der Universität Bonn, Germany
[3] Petersburg Nuclear Physics Institute, Gatchina, Russia
[4] Physikalisches Institut, Universität Erlangen, Germany
[5] KVI, University of Groningen, The Netherlands
[6] Department of Physics, Florida State University, Tallahassee, USA
[7] Physikalisches Institut, Ruhr-Universität Bochum, Germany
[8] Physikalisches Institut, Universität Basel, Switzerland
[9] II. Physikalisches Institut, Universität Giessen, Germany

Abstract. The beam asymmetry, Σ, was measured at ELSA in the reaction $\gamma\,p \to \eta\,p$ using linearly polarised tagged photon beams, produced by coherent bremsstrahlung off a diamond. The crystal was oriented to provide polarised photons in the energy range $E_\gamma = 800$ to 1400 MeV with the maximum polarisation of $P_\gamma = 49\,\%$ obtained at 1305 MeV. Both dominant decay modes of the η into two photons and $3\pi^0$ were used to extract the beam asymmetry from the azimuthal modulation of the cross section. The measurements cover the angular range $\Theta_{\mathrm{cm}} \simeq 50$ – 150 degrees. Large asymmetries up to $80\,\%$ are observed, in agreement with a previous measurement. The `eta-MAID` model and the Bonn–Gatchina partial wave analysis describe the measurements, but the required partial waves differ significantly.

PACS. 13.60.-r Photon and charged-lepton interactions with hadrons – 13.60.Le Meson production – 13.88.+e Polarization in interactions and scattering – 14.20.Gk Baryon resonances with S=0

1 Introduction

The rich excitation spectrum of the nucleon mirrors its complicated multi–quark inner dynamics. Therefore baryon spectroscopy is expected to provide benchmark data for any model of the nucleon, e.g. quark models in their variety [1,2] or, increasingly in the near future, Lattice QCD as an approximation of full Quantum Chromodynamics [3]. However, in many cases widths and density of states prohibit a clean identification, i.e. an unambiguous assignment of quantum numbers within a partial wave analysis.

The analyses are mostly based on pion and kaon induced reactions. Since some excited states are suspected to have a strongly disfavoured πN coupling [4], photoinduced reactions offer a complementary access to the nucleon spectrum, in particular in non-pionic final states. This provided the motivation to search for expected (within quark models) but yet unobserved "missing" resonances in η photoproduction off the proton [5,6,7].

a present address: University of South Carolina, USA
b present address: University of South Carolina, USA
c present address: University of Mainz, Germany
d on leave from Nucl. Phys. Division, BARC, Mumbai, India
e present address: FZ Jülich, Germany
f present address: University of Münster, Germany
Correspondence to: H. Schmieden, Nussallee 12, 53115 Bonn, Germany, e-mail: schmieden@physik.uni-bonn.de

The η channel provides a great simplification to the complex spectrum. Due to its isospin $I = 0$ it only connects N^* states ($I = 1/2$) to the nucleon ground state, but no Δ states ($I = 3/2$). Nevertheless, an unambiguous extraction of all contributing partial waves still requires a complete experiment with respect to the reaction amplitudes. Pseudoscalar meson photoproduction is determined by 4 complex amplitudes. However, due to the inherent nonlinearities it is not sufficient to measure $8 - 1$(overall phase) $= 7$ independent quantities, as could be naively expected. Instead, it can be shown that a minimum of 8 observables needs to be measured [8]. Besides the differential cross section those include 3 single-spin and 4 double-spin observables. The combination of double-spin observables can be appropriately chosen, but cross section, target asymmetry, T, recoil polarisation, P, and beam asymmetry, Σ, are required in any case (for a definition of the observables see e.g. ref.[9]).

Once a linearly polarised photon beam is provided, the photon-beam asymmetry is already accessible without polarised target or recoil polarimetry. For this case the cross section of pseudoscalar meson photoproduction off a nucleon can be cast into the form [9]

$$\frac{d\sigma}{d\Omega} = \frac{d\sigma_0}{d\Omega} \left(1 + P_\gamma \, \Sigma \, \cos 2\Phi\right), \qquad (1)$$

where σ_0 denotes the polarisation independent cross section, P_γ the degree of linear polarisation of the incident photon beam, and Φ the azimuthal orientation of the reaction plane with respect to the plane of linear polarisation. While in principle it suffices to determine $d\sigma/d\Omega$ around $\Phi = 0$ and $\Phi = 90$ degrees, it is more favourable to extract the beam asymmetry from the modulation of the cross section over the full azimuthal circle, since systematic effects are better under control. Thus, a cylindrically symmetric detector such as Crystal Barrel [10] is particularly suited to measure Σ in η photoproduction.

Most previous experiments investigated differential cross sections [5,11,12,13]. But there are also a few measurements of single polarisation observables. Heusch et al. [14] determined the recoil proton polarisation in η photoproduction between 0.8 GeV and 1.1 GeV in a spark chamber experiment. The target asymmetry was measured at the Bonn synchrotron [15]. A first measurement of the photon beam asymmetry using linearly polarised photon beams was accomplished at the laser backscattering facility GRAAL at the ESRF Grenoble [16]. The GRAAL experiments were later on extended to higher energies and preliminary results have been presented at conferences [17]. Large $\Sigma \simeq 0.5$ were obtained in the near-threshold region. Contrary, in η electroproduction the TT interference cross section, which is related to Σ, was found consistent with zero over almost all the range in $Q^2 = 0.25 - 1.5$ GeV/c^2 in the threshold region [18].

In order to clarify this situation and to extend the energy range in η photoproduction we carried out experiments with linearly polarised tagged photon beams at the electron accelerator ELSA [19] of the University of Bonn. The following section is first devoted to the experimental setup. In addition to the basic analysis steps, section 3
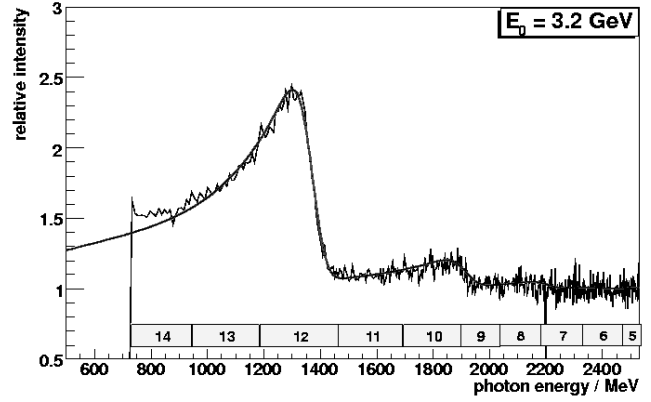

Fig. 1. The measured coherent bremsstrahlung intensity normalised to an incoherent spectrum (histogram, see text) in comparison to an improved version [21] of the ANB-calculation [22] (full curve). The diamond radiator was set for an intensity maximum at $E_\gamma = 1305$ MeV. The numbered blocks indicate the ranges covered by the 14 timing scintillators of the tagging detector.

then describes the method of extracting Σ. The results are discussed in section 4 and, after a brief summary, tabulated in the appendix.

2 Experimental Setup

Electron beams of $E_0 = 3.2$ GeV were used to produce coherent bremsstrahlung from a $500\,\mu$m thick diamond crystal. Electrons which radiated a photon are momentum analysed using a magnetic dipole (tagging-) spectrometer. Its detection system consists of 14 plastic scintillators providing fast timing and additional hodoscopes to achieve the required energy resolution: The range of low electron energies, corresponding to $E_\gamma = 0.8...0.92\,E_0$, is covered by a multi-wire proportional chamber, a 480 channel double-layer scintillating fibre detector complements the range $0.18...0.8\,E_0$. At the nominal setting of $E_0 = 3.2$ GeV the energy resolution varies between 2 MeV for the high photon energies and 25 MeV for the low energies. Since the photon beam remained virtually uncollimated, the measured electron spectrum directly reflects the photon spectrum.

Fig.1 shows the photon energy distribution obtained from the diamond radiator, measured through the detection of the corresponding electrons in the tagging system. This spectrum is normalised to the spectrum of an amorphous copper radiator. Hence, a constant run of the curve corresponds to the ordinary $\sim 1/E_\gamma$ dependence in the bremsstrahlung process. This representation accentuates the coherence effect, which manifests itself in clear peaks. Within the range of the coherent peaks the bremsstrahlung recoil is transferred to the whole crystal as opposed to individual nuclei in the incoherent process, thus fixing the plane of electron deflection very tightly relative to the orientation of the crystal lattice. Consequently, the emitted photons are linearly polarised [20].
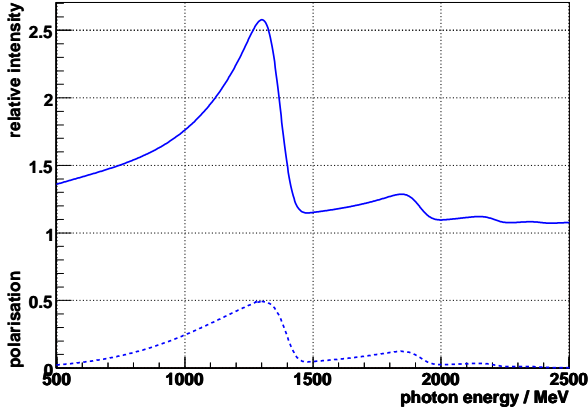
Fig. 2. Calculation of relative bremsstrahlung intensity (top curve) and corresponding degree of linear polarisation (bottom curve) using an improved version [21] of the ANB bremsstrahlung code [22] with scaled incoherent contribution (see text). A scaling factor of 1.35 is used to achieve best agreement with the measured spectra (cf. Fig. 1).

Fig. 3. Setup of the detector system as described in the text. The photon beam enters from left.

The maximum achievable degree of polarisation decreases with increasing photon energy, $P_\gamma \simeq 0.4$ is obtained at $E_\gamma = E_0/2$. The orientation of the linear polarisation and the position of the maximum in the photon energy-spectrum can be deliberately chosen through appropriate alignment of the crystal relative to the electron beam direction. We used a crystal setting to obtain the polarisation maximum at 1305 MeV. Vertical orientation of the polarisation vector was chosen, since the vertical emittance of the electron beam is about an order of magnitude better than in horizontal direction. A dedicated commercial 5-axis goniometer[1] enabled the accurate crystal alignment with typical angular uncertainties of $\delta < 170\,\mu$rad.

The curve in Fig.1 represents a calculation of the spectrum using an improved version [21] of the original ANB ("analytic bremsstrahlung calculation") software [22] from Tübingen University. It nicely describes the measured spectrum. This level of agreement can be only obtained, if the *incoherent* part of the ANB calculation is scaled by a factor of 1.35. This was traced back to an inaccurate inclusion of multiple scattering and an uncertainty in the atomic form factors [21]. Using the form factor parametrisation after Schiff [23] instead that of Hubbell [24] improves the agreement significantly.

The relative strengths of coherent and incoherent contributions determine the absolute value of linear polarisation. It can be obtained from *any* fit of the spectrum as long as there is no overlap of different reciprocal lattice vectors — which can correspond to different orientations of the resulting polarisation vector — within a given energy interval. This condition is surely fulfilled, if adjacent peak regions do not overlap. In this respect the mentioned re-scaling of the incoherent contributions introduces no significant error. As can be seen from Fig.1, in our particular case there is only a tiny overlap between the adjacent
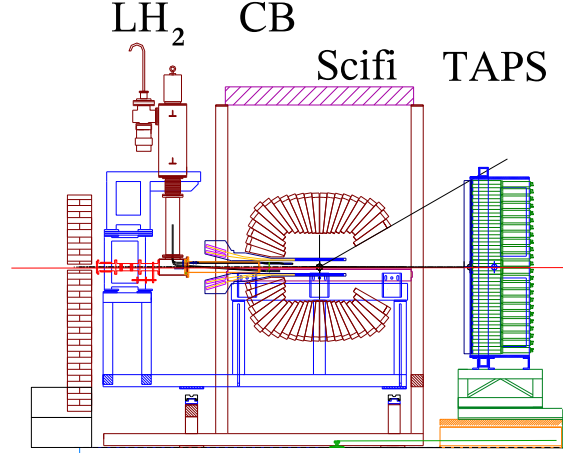
---

[1] *Newport* company

peaks. Furthermore, both of them even result in the same orientation of the polarisation vector.

Fig.2 shows the ANB-calculated relative photon intensity spectrum in conjunction with the calculated photon polarisation. The maximum polarisation of $P_\gamma = 0.49$ is obtained at $E_\gamma = 1305$ MeV, as expected. An absolute error of $\delta P_\gamma < 0.02$ is estimated. The total photon flux was up to 2×10^7 s^{-1}.

The detector setup of the experiment is depicted in Fig.3. The linearly polarised photon beam was incident on a 5.3 cm long liquid hydrogen target with $80\,\mu$m Kapton windows [25]. A three layer scintillating fibre detector [26] surrounded the target within the polar angular range from 15 to 165 degrees. It determined a piercing point for charged particles. Both, charged particles and photons were detected in the `Crystal Barrel` detector [10]. It was cylindrically arranged around the target with 1290 individual CsI(Tl) crystals in 23 rings, covering a polar angular range of 30 — 168 degrees. The crystals of 16 radiation lengths guaranteed nearly full longitudinal shower containment. In transverse direction electromagnetic showers extended over up to 30 modules. For photons an energy resolution of $\sigma_{E_\gamma}/E_\gamma = 2.5\,\%/^4\sqrt{E_\gamma/\mathrm{GeV}}$ and an angular resolution of $\sigma_{\Theta,\Phi} \simeq 1.1$ degree was obtained.

The 5.8 — 30 degree forward cone was covered by the `TAPS` detector [27], set up in one hexagonally shaped wall of 528 BaF$_2$ modules. For photons between 45 and 790 MeV the energy resolution is $\sigma_{E_\gamma}/E_\gamma = \left(0.59/\sqrt{E_\gamma/\mathrm{GeV}} + 1.9\right)\%$ [28]. The position of photon incidence could be resolved within 20 mm. For charged particle recognition each `TAPS` module has a 5 mm plastic scintillator in front of it.

In contrast to `Crystal Barrel`, the fast `TAPS` detectors are individually equipped with photomultiplier readout. Thus, the first level trigger was derived from `TAPS`, requiring either ≥ 2 hits above a low threshold (A) or, alternatively, ≥ 1 hit above a high threshold (B). Using, within $\simeq 10\,\mu$s, a fast cluster recognition [29] for the `Crystal`
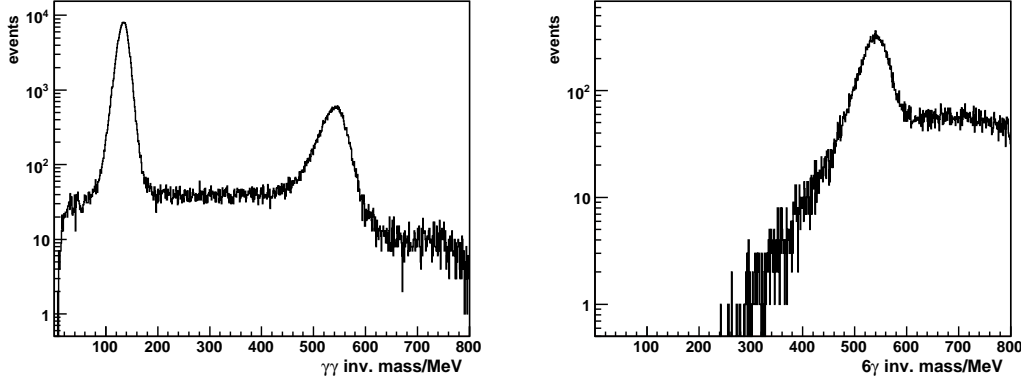
Fig. 4. Invariant mass distribution after standard kinematic analysis cuts. Left: Two photon invariant mass distribution for the 3–cluster data set; signal widths of $\sigma_{\pi^0} = 10$ MeV and $\sigma_\eta = 22$ MeV are obtained. Right: 6 photon invariant mass distribution for the 7–cluster data set with $\sigma_\eta = 25$ MeV. Note the logarithmic scale.

Barrel as second level trigger (C), the total trigger condition required $[A \vee (B \wedge C)]$, with 2 clusters identified at second level.

3 Event reconstruction and data analysis

To enrich the $\eta\,p$ final state, the occurence of, in total, either three or seven detector hits was required during the offline analysis, corresponding to two or six photons and the proton. In particular photon hits usually fire a cluster of adjacent crystals whose energy is summed over. After the basic detector calibrations from the data itself, the η meson is identified in either of its major decay modes into two photons or $3\pi^0$. Fig. 4 shows the respective invariant mass distributions, obtained after only basic kinematic cuts have been applied in order to ensure consistence of the azimuthal angles (i.e. coplanarity) and polar angles involved. No cuts were applied on the energy of the respective hit of the proton candidate. The signal widths in Fig. 4 are $\sigma_{\eta\to\gamma\gamma} = 22$ MeV and $\sigma_{\eta\to3\pi^0} = 25$ MeV, respectively. To avoid any possible bias from detector inefficiencies on the azimuthal distributions, the proton was *not* positively identified by using the signals of the inner scintillating fibre detector of the barrel or the veto detectors of TAPS. Instead, all combinatorial possibilities were processed, i.e. 3 for the 3–cluster events and 21 for the 7–cluster events. A cut on the missing mass applied to the proton candidates subsequently yielded a clean separation. No kinematic fit was used to improve the separation, nor to increase the resolution.

As can be seen from Fig. 4, the background below the η peaks is very small (note the logarithmic scale). It varies with photon energy and thus was determined in each bin of E_γ. Two different fits were used to interpolate the background between the edges of the signal, linear and gaussian. From the difference the possible systematic error was estimated which may be due to the background subtraction scheme.
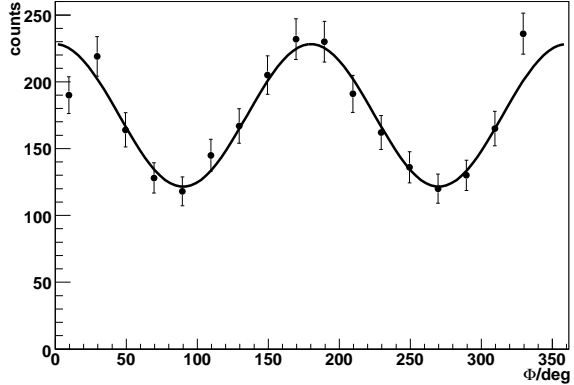

Fig. 5. Example of a measured Φ distribution in the bin $E_\gamma = 1240 — 1350$ MeV and $\Theta_{\mathrm{cm}} = 66 — 92$ degrees for the $\eta \to 2\gamma$ decay channel. The event-weighted average polarisation was $P_\gamma = 47.3\,\%$.

3.1 Beam asymmetry

Cuts of 3σ widhts around the η–mass in the invariant mass spectra (Fig. 4) yielded a clean event sample. To extract the photon beam asymmetry according to Eq. 1, a fit of the azimuthal event distribution was performed:

$$f(\Phi) = A + B\,\cos(2\Phi). \tag{2}$$

An example for one bin in E_γ and Θ^{cm} is shown in Fig. 5. The ratio B/A of the fit determines the product of beam asymmetry and photon polarisation, $P_\gamma \Sigma$, of Eq. 1. Since there is a strict relation between the photon energy and the photon polarisation (c.f. Fig. 2), and the appropriate photon energy can be assigned to each single event, it is possible to determine the event-weighted average polarisation in each bin of photon energy.

The photon asymmetries extracted from the $\eta \to 2\gamma$ and the $\eta \to 3\pi^0$ decay channels agree very well. This

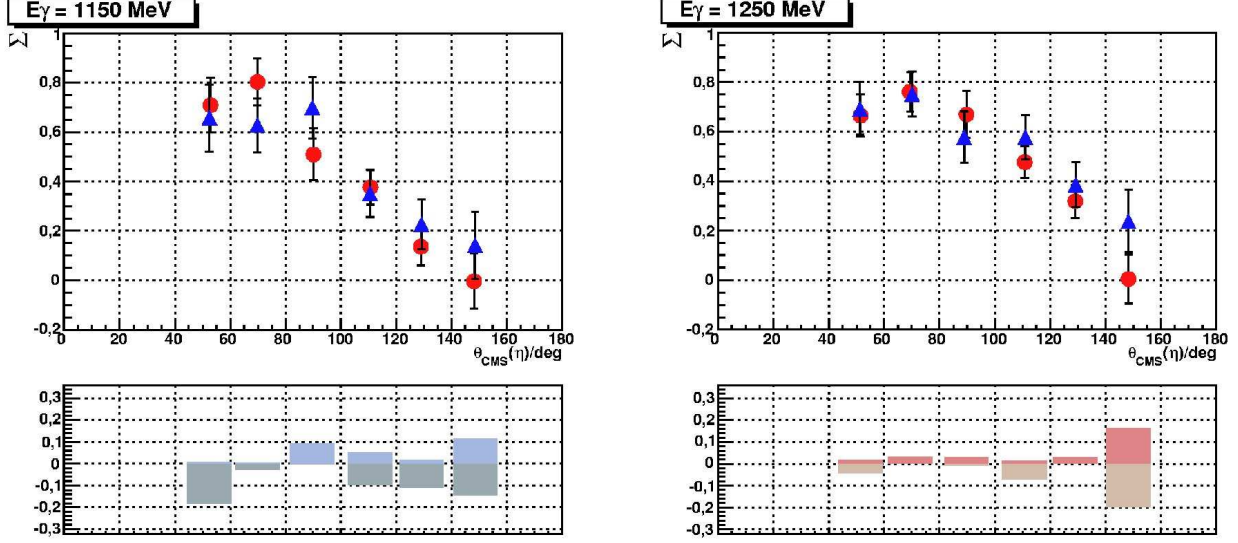**Fig. 6.** Measured photon asymmetry, Σ, as extracted from the decay channels $\eta \to 2\gamma$ (dots) and $\eta \to 3\pi^0$ (triangles) for the two photon energy bins 1150 MeV (left) and 1250 MeV (right). The bar charts indicate the total fluctuation (*no 1–σ errors*) of Σ if extracted from the Φ ranges 0 — 180 degrees (light) and 180 — 360 degrees (dark) seperately, instead of using the full range. Bottom left is for the $\eta \to 3\pi^0$ channel in the 1150 MeV bin, bottom right for the $\eta \to 2\gamma$ mode in the 1250 MeV bin.

is illustrated in Fig. 6 (top) where, as examples, the two photon energy bins 1150 ± 50 MeV (left) and 1250 ± 50 MeV (right) are shown.

In order to detect possible false detector asymmetries, the uniformity of the event distribution of the laboratory angles Θ versus Φ was routinely inspected [21]. Most detected problems could be removed in the offline analysis. Other sources of false asymmetries were identified but could not be completely remedied, e.g. trigger inefficiencies within certain angular regions. In such bins the corresponding Φ–regions were excluded from the fit of Eq. 2. The remaining systematic error is estimated through the difference of separate fits of the 0 — 180 and 180 — 360 degree azimuthal regions to the full fit. The differences are shown as the bar graphs on the bottom of Fig. 6, left in the 2γ, right in the $3\pi^0$ decay of the η meson. Note that these estimates are correlated with the statistical errors.

It turned out that the angle dependent inefficiencies provide by far the major contribution to the systematic error of this experiment. In contrast, the remaining uncertainty of the beam polarisation affects the final result much less, and the effect of the background subtraction is almost negligible. The total error remains, however, still dominated by statistics as can also be seen from the table of results in the appendix.

4 Results and discussion

The combined results of the $\eta \to 2\gamma$ and $\eta \to 3\pi^0$ data sets are presented in Fig. 7. Statistical errors are directly attached to the data points. Since determined from the χ^2 of the fit of Eq. 2, these statistical errors may still carry some correlation to systematics. The estimated total systematic uncertainty is indicated by the bars.

Nice agreement is found with the published GRAAL data of Ajaka et al. [16]. This provides confidence that the analysis chain is well under control on the level of the presented errors, in particular the determination of the degree of linear polarisation and the extraction of the azimuthal asymmetries, the latter despite the fact that, due to the unfavourable horizontal beam emittance, no data were taken with the polarisation plane rotated by 90 degrees, as was done by the GRAAL collaboration. More recent but yet preliminary (and hence here not shown) data of the GRAAL collaboration, extended in energy up to 1445 MeV [17], do also nicely agree with our data.

In Fig.7 our new data are compared to two standard calculations, the Mainz isobar model `eta-MAID` [30] and the Bonn–Gatchina partial wave analysis `BnGa` [31]. In contrast to `eta-MAID`, the Bonn–Gatchina analysis in addition to ηN also takes the πN, $K\Lambda$ and $K\Sigma$ coupled channels into account. To calculate the photon asymmetry, the preliminary high energy GRAAL data [17] have already been used in the `BnGa` fit. This might be the reason for the slightly better description of our data.

The overall agreement between data and both models seems very satisfactory at first glance. Closer examination reveals distinct inconsistencies, however. While the full model results agree, the individual resonance contributions differ substantially as is illustrated in Fig. 8.

Within the energy range considered, the tail of the $S_{11}(1535)$ state provides an important contribution to the cross section in both models. In `eta-MAID` the $P_{11}(1710)$ is required as well to describe the cross section, whereas the `BnGa` PWA prefers a strong $P_{13}(1720)$ partial wave. This also shows up in the photon asymmetry. The $P_{11}(1710)$ (long dashed-dotted) affects Σ in `eta-MAID`, albeit weakly. No impact at all is found in the `BnGa` PWA. In contrast,
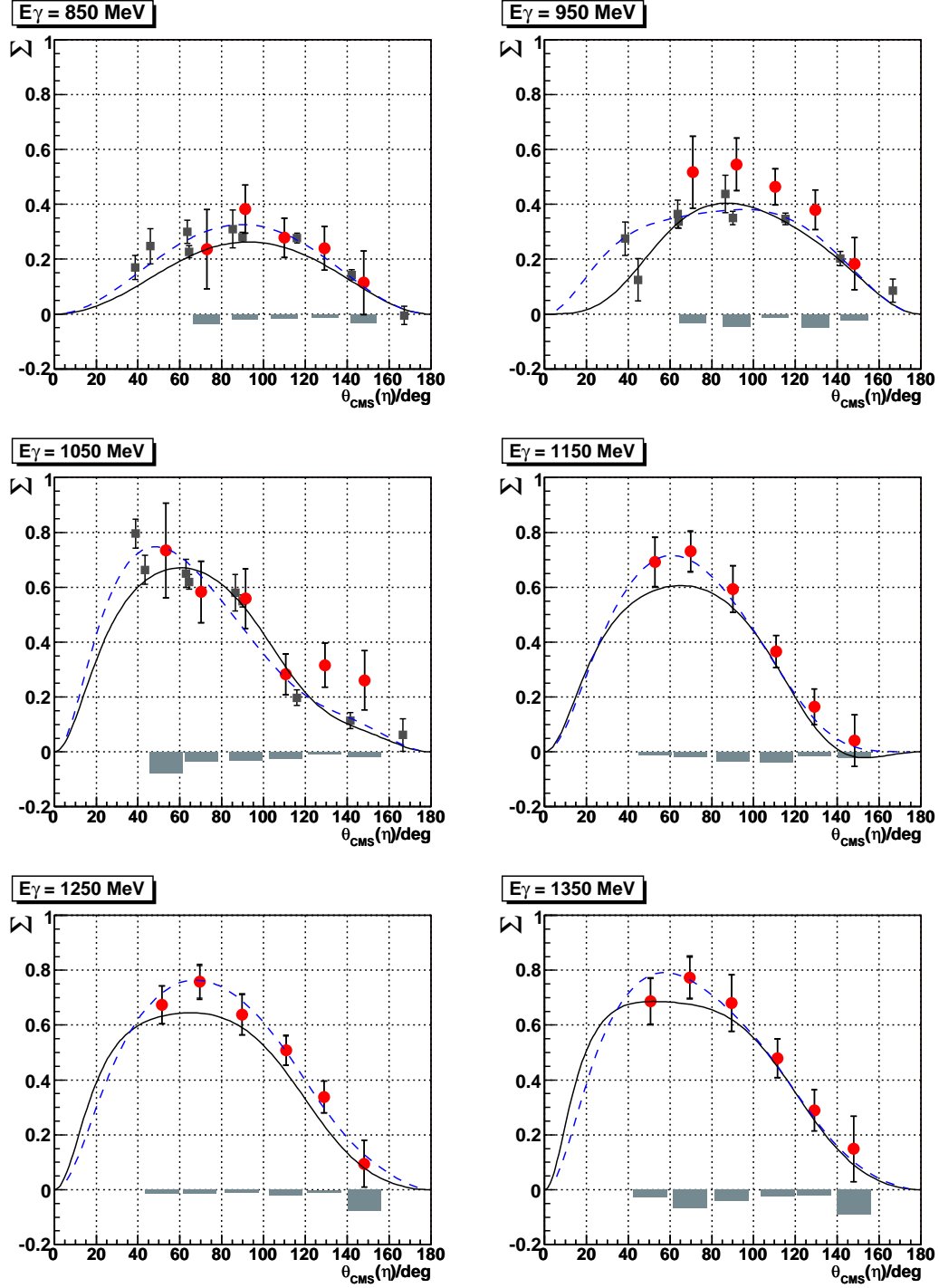
Fig. 7. Photon asymmetry from the combined η decay modes (filled circles) with statistical errors. The systematical error is indicated by the bar chart. Our results are compared to the published data (boxes) of the GRAAL collaboration [16] (see also text). The curves represent calculations of `eta-MAID` [30] (full) and the Bonn–Gatchina partial wave analysis `BnGa` [31] (dashed).
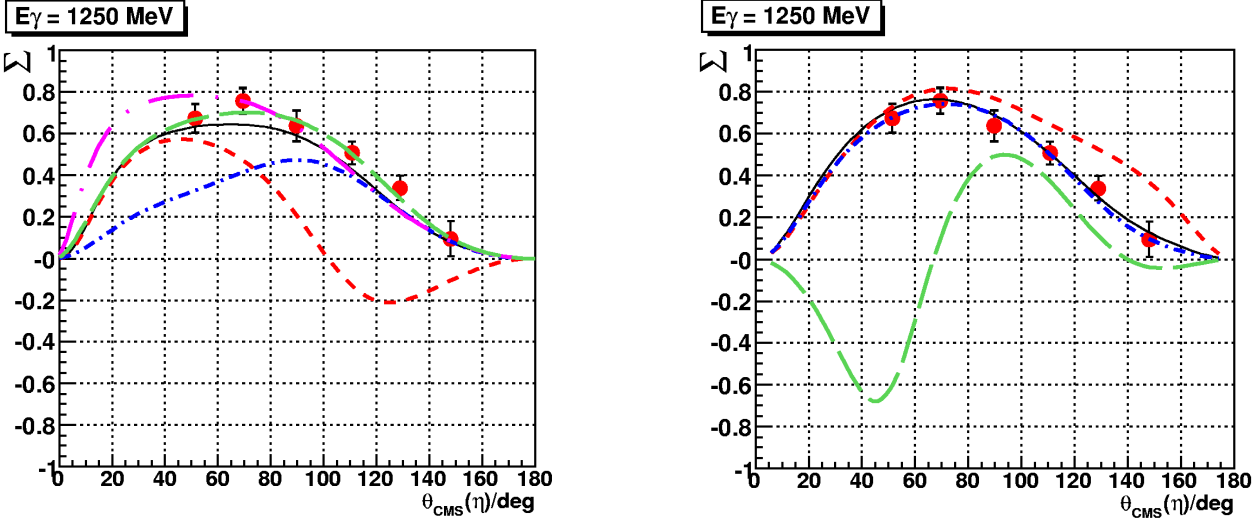
Fig. 8. Sensitivity of the `eta-MAID` and the `BnGa` calculations to different resonance contributions in the energy bin $E_\gamma = (1250 \pm 50)$ MeV. Data points are the same as in Fig. 7. Left the `eta-MAID` result [30] is shown, right the `BnGa` analysis [31]. The full lines represent the respective full calculations. The broken curves illustrate the impact of "turning off" individual resonances: Long dashed without $P_{13}(1720)$, long dashed-dotted without $P_{11}(1710)$ (no difference to full calculation in `BnGa` analysis), short dashed without $D_{13}(1520)$, and short dashed-dotted without $D_{15}(1675)$.

the influence of the $P_{13}(1720)$ (long dashed) on the photon asymmetry is pronounced only in the `BnGa` model. Within `eta-MAID`, turning off the $P_{13}(1720)$ leaves the photon asymmetry almost unaffected. Both the $D_{13}(1520)$ (short dashed) and $D_{15}(1675)$ (short dashed-dotted) states have a strong influence on Σ within `eta-MAID`. Contrary, the $D_{15}(1675)$ remains negligible in the `BnGa` calculation; the $D_{13}(1520)$ has a weak impact but, compared to `eta-MAID`, in opposite direction (cf. Fig. 8).

This unsatisfactory situation can not be resolved from measurements of the photon asymmetry alone. Yet, such data provide the necessary basis to be extended with double polarisation observables in order to get closer to, or even accomplish the complete experiment in terms of the introductory discussion.

5 Summary and conclusions

In summary, we have presented data on the photon beam asymmetry, Σ, in the reaction $\gamma + p \rightarrow p + \eta$. The continuous 3.2 GeV ELSA electron beam was used to produce a linearly polarised tagged photon beam by means of coherent bremsstrahlung off a diamond crystal, covering a photon energy range $E_\gamma = 800...1400$ MeV with polarisation degrees up to 49 %. A combined setup of the `Crystal Barrel` and `TAPS` detectors enabled high-resolution detection of multiple photons, important for the clean detection of the 2γ and $3\pi^0$ decays of the η meson. We obtained photon asymmetries in excess of 50 % in some angular and energy bins. The results are in agreement with a previous measurement by the GRAAL collaboration in the overlapping energy intervals. The `eta-MAID` model and the Bonn–Gatchina partial wave analysis provide a satisfactory overall description of our data. In detail, however,

there are marked differences with regard to the role of individual resonance contributions. To resolve this problem, further double-polarisation experiments are indispensable. They will be tackled at several laboraties, at ELSA within the Collaborative Research Project SFB/TR-16 with use of the Bonn polarised solid state target.

Appendix

The detailed results of the photon asymmetries, Σ, from the reaction $\gamma p \rightarrow \eta p$ are summarised in Table 1. To each value of the photon asymmetry is assigned the corresponding 1-σ statistical error and an 1-σ estimate of the total systematical error.

energy bin **850** MeV

E_γ/MeV	θ_η^{cm}	Σ	$\sigma(\Sigma)_{stat}$	$\sigma(\Sigma)_{sys}$
843.4	72.9	0.237	0.145	0.036
842.6	91.2	0.382	0.087	0.020
846.4	109.9	0.278	0.071	0.015
847.5	129.2	0.240	0.079	0.012
850.5	147.9	0.114	0.116	0.031

energy bin **950** MeV

E_γ/MeV	θ_η^{cm}	Σ	$\sigma(\Sigma)_{stat}$	$\sigma(\Sigma)_{sys}$
942.8	70.9	0.517	0.131	0.033
939.7	91.9	0.546	0.095	0.045
941.7	110.3	0.465	0.065	0.013
943.6	129.4	0.380	0.072	0.049
943.8	148.2	0.184	0.095	0.023

energy bin **1050** MeV

E_γ/MeV	θ_η^{cm}	Σ	$\sigma(\Sigma)_{stat}$	$\sigma(\Sigma)_{sys}$
1054.0	53.3	0.734	0.172	0.077
1051.2	70.1	0.583	0.111	0.035
1046.0	91.4	0.559	0.108	0.032
1045.9	110.6	0.283	0.074	0.023
1043.0	129.4	0.316	0.080	0.010
1043.3	148.4	0.261	0.107	0.019

energy bin **1150** MeV

E_γ/MeV	θ_η^{cm}	Σ	$\sigma(\Sigma)_{stat}$	$\sigma(\Sigma)_{sys}$
1154.4	52.9	0.692	0.090	0.013
1151.5	69.8	0.731	0.072	0.019
1150.2	90.1	0.593	0.084	0.036
1151.4	110.7	0.366	0.058	0.037
1150.0	129.0	0.165	0.064	0.014
1148.5	148.2	0.041	0.095	0.020

energy bin **1250** MeV

E_γ/MeV	θ_η^{cm}	Σ	$\sigma(\Sigma)_{stat}$	$\sigma(\Sigma)_{sys}$
1251.4	51.5	0.674	0.068	0.016
1249.3	69.4	0.758	0.060	0.017
1249.0	89.8	0.638	0.073	0.012
1249.5	110.7	0.508	0.053	0.021
1249.5	129.0	0.338	0.058	0.010
1250.0	148.2	0.095	0.085	0.076

energy bin **1350** MeV

E_γ/MeV	θ_η^{cm}	Σ	$\sigma(\Sigma)_{stat}$	$\sigma(\Sigma)_{sys}$
1344.7	50.7	0.687	0.083	0.027
1343.5	69.4	0.774	0.075	0.069
1342.4	89.4	0.680	0.102	0.043
1342.6	111.3	0.479	0.070	0.026
1343.4	129.0	0.290	0.075	0.021
1343.1	147.9	0.149	0.119	0.089

Table 1. Photon asymmetries for the reaction $\gamma p \to \eta p$. Angles are given in degrees. Energy-bin widths are ± 50 MeV.

References

1. see e.g. S. Capstick and W. Roberts, Prog. Part. Nucl. Phys. **45** (2000) 241
2. U. Löring et al., Eur. Phys. J. **A10** (2001) 395, 447
3. A.C. Kalloniatis, D.B. Leinweber, A.G. Williams (Eds.), "Lattice Hadron Physics", Lecture Notes in Physics **663**, Springer (2005)
4. S. Capstick and W. Roberts, Phys. Rev. **D 49** (1994) 4570
5. V. Crede et al., Phys. Rev. Lett. **94** (2005) 012004
6. B. Saghai and Z. Li, Proceedings of the Workshop on the Physics of excited Nucleons, Pittsburgh (2002), ed. by S.A. Dytman and E.S. Swanson (World Scientific, 2003), p. 166
7. G.Y. Chen eta al., Nucl. Phys. **A723** (2003) 447
8. W.-T. Chiang and F. Tabakin, Phys. Rev. **C55** (1997) 2054
9. G. Knöchlein, D. Drechsel and L. Tiator, Z. Phys. **A352** (1995) 327
10. E. Aker et al., Nucl. Instr. Meth. **A321** (1992) 69
11. B. Krusche et al., Phys. Rev. Lett. **74** (1995) 3736
12. F. Renard et al., Phys. Lett. **B528** (2002) 215
13. M. Dugger et al., Phys. Rev. Lett. **89** (2002) 22202 and 249904(E)
14. C. A. Heusch et al., Phys. Rev. Lett. **25** (1970) 1381
15. A. Bock et al., Phys. Rev. Lett. **81** (1998) 534
16. J. Ajaka et al., Phys. Rev. Lett. **81** (1998) 1797
17. V. Kouznetsov et al., *PIN* Newsletter **16** (2002) 160
18. R. Thompson et al., Phys. Rev. Lett. **86** (2001) 1702
19. W. Hillert, Eur. Phys. J. **A28**, s01 (2006) 139
20. U. Timm, Fortschritte der Physik **17** (1969) 765
21. D. Elsner, doctoral thesis, Bonn (2006)
22. F.A. Natter et al., Nucl. Instr. Meth. **B211** (2003) 465
23. L.I. Schiff, Phys. Rev. **83** (1951) 252
24. J.H. Hubbell, J. Appl. Phys. **30** (1959) 981
25. B. Kopf, doctoral thesis, Dresden (2002)
26. G. Suft et al., Nucl. Instr. Meth. **A538** (2005) 416
27. R. Novotny et al., IEEE transaction on nuclear science **38** (1991) 378
28. A.R. Gabler et al., Nucl. Instr. Meth. **A346** (1994) 168
29. H. Flemming, doctoral thesis, Bochum (2000)
30. W.T. Chiang, S.N. Yang, L. Tiator, D. Drechsel, Nucl. Phys. **A700** (2002) 429;
   see also `http://www.kph.uni-mainz.de/MAID/maid.html`
31. A.V. Anisovich et al., Eur. Phys. J. **A25** (2005) 427